Nuclear Materials and Energy 15 (2018) 226–231

Contents lists available at ScienceDirect

Nuclear Materials and Energy

journal homepage: www.elsevier.com/locate/nme

Oxidation resistance of bulk plasma-facing tungsten alloys

F. Klein[*,a], T. Wegener[a], A. Litnovsky[a], M. Rasinski[a], X.Y. Tan[a,b], J. Gonzalez-Julian[a], J. Schmitz[a,c], M. Bram[a], J.W. Coenen[a], Ch. Linsmeier[a]

[a] Forschungszentrum Jülich GmbH, Institut für Energie- und Klimaforschung, Jülich 52425 Germany
[b] School of Materials Science and Engineering, Hefei University of Technology, Hefei 23009, China
[c] Department of Applied Physics, Ghent University, 9000 Ghent, Belgium

ARTICLE INFO

Keywords:
W-based alloys
W–Cr–Y alloys
Oxidation resistance
DEMO

ABSTRACT

Tungsten (W) currently is the main candidate as plasma-facing armour material for the first wall of future fusion reactors, like DEMO. Advantages of W include a high melting point, high thermal conductivity, low tritium retention, and low erosion yield. However, in case of an accident, air ingress into the vacuum vessel can occur and the temperature of the first wall can reach 1200 K to 1450 K due to nuclear decay heat. In the absence of cooling, the temperature will remain in that range for several weeks. At these temperatures the radioactive tungsten oxide volatilizes. Therefore, 'smart' W alloys are developed that aim to preserve the properties of W during plasma operation coupled with suppressed tungsten oxide formation in case of an accident.

This study focusses on oxidation studies at 1273 K of samples produced by mechanical alloying followed by field assisted sintering. In a first step the sintering is optimized for tungsten (W) – chromium (Cr) -yttrium (Y) alloys. It is shown that the best oxidation resistance is achieved with submicron grain sizes. This yields a closed, protective oxide layer. In a second step the influence of the grinding process during sample preparation is analysed. It is shown that scratches initiate failure of the protective oxide. In a third step the oxidation and sublimation is measured for weeks – for the first time the sublimation is directly measured in order to determine the potential hazard in comparison to pure W. It is shown that the oxidation is suppressed in comparison to pure W. However, sublimation at a rate of 1×10^{-6} mg cm^{-2} s^{-1} starts after a few days. Nevertheless, the progess in smart alloys is evident: sublimation is delayed by about two days and complete mechanical destruction of the first wall is avoided.

1. Introduction

The future DEMOnstration power plant (DEMO) aims to demonstrate the technological and economical feasibility of fusion as a future energy source. This implies that the power plant must be safe. This is very challenging as the plasma facing components will have to withstand an unprecedented fluence of particles, radiation, and neutrons. These conditions make tungsten (W) a prime candidate as plasma facing material. Advantages include a low sputtering yield by plasma particles, a good thermal conductivity, a low tritium retention, and a high melting temperature [1–3]. Further, the radioactive isotopes, which are generated by neutron irradiation, decay to shielded hands-on level within 100 years [4].

One important safety criterion is that there should be full passive safety in a Loss-of-Coolant-Accident (LOCA) with simultaneous air ingress. During operation neutrons activate the W, as soon as the cooling system fails it heats up due to its nuclear decay heat. Modelling predicts a temperature rise to 1200 K to 1450 K where it remains for around 100 days [5]. In the presence of air, which may penetrate the vacuum vessel through leaks, the W oxidises rapidly at such temperatures. It forms radioactive WO_3 which then sublimates. Several hundred kg week^{-1} sublimate at 1273 K and above [6]. On top of that, W, WO_3 have a Pilling-Bedworth ratio (V_{oxide}/V_{metal}) of 3.4 [7]. This can cause strong tensions, breaking the W and detaching it from the first wall.

The aim is to overcome these problems by developing a new W alloy. On the one hand it must retain the beneficial properties of W for operation of the power plant. On the other hand it must form a protective layer in case of a loss-of-coolant accident coupled with air ingress. This protective layer shall fulfill two goals: firstly, the formation of WO_3 must be suppressed so that no radioactive W is released to the environment. Secondly, the first wall shall not disassemble in an uncontrolled way and shall not pose additional challenges to potential emergency measures.

It was shown that alloys containing tungsten (W), 11.4 weight (

* Corresponding author.
E-mail address: fe.klein@fz-juelich.de (F. Klein).

https://doi.org/10.1016/j.nme.2018.05.003
Received 29 November 2017; Received in revised form 13 April 2018; Accepted 8 May 2018

wt.) % chromium (Cr), and 0.6 wt. % yttrium (Y) are a promising candidate [8–10]. In the following this is written as W-11.4Cr-0.6Y. The Cr was found to form a protective oxide scale on the surface suppressing the formation of WO_3. The Y was found to be crucial to support the formation of this protective oxide scale. However, these studies were conducted with thin films on the timescale of a few hours. This study aims at investigating the oxidation and sublimation behaviour of these alloys over several weeks – a timescale relevant for DEMO. This requires a large material reservoir. One option for compacting bulk samples is Field Assisted Sintering Technology (FAST). In a first step, different FAST parameters are tested to sinter the novel W–Cr–Y alloys. In a second step, the influence of the grinding process in the surface of the sintered samples is studied. In a third step, the oxidation and sublimation characteristics for weeks in synthetic air at 1273 K are studied.

2. Experimental

To start bulk sample production, W, Cr, and Y powders are mixed and milled in a planetary ball mill, Retsch PM400. After 60 h of milling a homogeneous powder is achieved – more details on the mechanical alloying procedure can be found in ref. [9]. Consolidation is achieved by Field Assisted Sintering Technology (FAST), FCT HPD5, FCT Systeme GmbH [11]. The heating rate is chosen to be $100\,\mathrm{K\,min^{-1}}$ or $200\,\mathrm{K\,min^{-1}}$, and a maximum temperature in the range of 1700 K to 1850 K is selected. The powder is poured in a standard graphite tool of 20 mm inner diameter. Previously, a graphite foil is placed in the inner face of the die to ensure a good electrical, thermal, and mechanical contact. Sintering is achieved by applying an uniaxial pressure (50 MPa), and heating using a current generated by a DC pulse generator.

The obtained sample is cut using a diamond blade saw and ground using a planar grinding and polishing machine. Unless stated differently, the final grinding step is performed using a P1200-grade silicon carbide abrasive paper. Grinding creates a reproducible surface finish by removing the first 0.5 mm where carbon from the foil diffused during sintering.

The density of the samples is measured using Archimedes principle. The mass is measured using the Sartorius MSA225P micro-balance (resolution 10 µg), whereas the volume is determined by the mass of the displaced ethanol using the same micro-balance.

Oxidation is performed in a thermogravimetric analyser, the TAG-16/18 from Setaram. It allows to measure the in-situ mass change of a sample in a temperature range of 300 K to 2000 K. The drift of the scale for isothermal oxidations with the duration of several days is $2 \times 10^{-8}\,\mathrm{mg\,s^{-1}}$. This is possible due to a symmetrical, dual furnace design: one furnace contains the sample, the other furnace contains an inert product with the same volume to compensate buoyancy effects. The mass increase of the sample is measured by placing the sample into an alumina crucible which is attached to the balance by a platinum wire. The oxidation rate is determined by the mass increase of the sample as oxygen is added to the material.

The same device can also be used to measure sublimation. The sublimation rate provides an estimate for the radiological hazard. It is measured as illustrated in Fig. 1: an alumina tube is attached to the balance using a platinum wire. The sample hangs inside the tube attached to a second platinum wire. Thus, there is no direct contact between the sample and the tube at the balance. As soon as sublimation of the sample starts, part of the material will deposit onto the alumina tube and cause a mass increase which is measured. The present work assumes that all material deposits onto the alumina tube and that no material sublimates from the tube due to its high porosity. Thus, the given sublimation rates are a lower boundary.

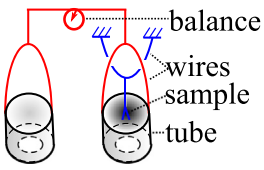

Fig. 1. Schematic of the sublimation measurement setup.

Electron microscopy provides insights into the grain structure and the structure and composition of the oxide layers. The combined Scanning Electron Microscopy (SEM) – Focussed Ion Beam (FIB) system Carl Zeiss CrossBeam XB540 equipped with an Energy Dispersive X-ray analysis (EDX) is used. The FIB allows to cut cross sections providing insights into the microstructure of a sample. During cutting the surface of the sample is damaged due to sputtering, therefore a layer of platinum (Pt) is deposited onto the sample before cutting.

The surface roughness is measured using the Dektak 6M from Bruker. A diamond-tipped stylus with a diameter of 2 µm is moved across the sample. The mechanical movement of the stylus yields a 2D surface profile.

3. Results

3.1. Material optimisation

There are four main methods to produce W–Cr–Y samples: Hot Isostatic Pressing (HIP) [12], pressureless sintering [13], Field Assisted Sintering Technology (FAST), and magnetron sputtering [6,8]. Magnetron sputtering allows quick production of a large number of samples. One obtains a thin film with a thickness of around 3.5 µm and a homogeneous distribution of W, Cr, Y, see Fig. 2a. The grain size is of around 0.1 µm. Fig. 2 e shows that this alloy forms a protective, closed Cr_2O_3 layer with some internal Cr_2O_3 when exposed to 1273 K at 20 kPa O_2 and 80 kPa Ar partial pressure. This protective oxide layer meets the main requirement – preventing the formation of WO_3.

However, due to the small thickness the material reservoir of thin films is small: bulk samples are required for long-term studies. This study employs FAST where sintering happens within minutes and grain growth can be controlled. The main parameters that can be tuned are the heating rate h, the maximum sintering temperature T_{max}, and the holding time t_{hold}.

The first samples are produced with $h = 200\,\mathrm{K\,min^{-1}}$, $T_{max} = 1823\,\mathrm{K}$, and $t_{hold} = 1\,\mathrm{min}$. A relative density of 98.5 % and large grains with a size of 1 µm is achieved. The oxidation performance is shown in Fig. 3: breakaway oxidation is found – breakaway oxidation is a short, temporal increase of the mass gain rate. The oxidation rate is still 1000 times slower than for pure W. However, further improvement is desired. Based on the experience with thin films, the following production steps aim at achieving a smaller grain size.

A smaller grain size can be achieved by reducing the sintering temperature T_{max} as grain growth slows down at lower temperatures. Different samples are prepared with fixed $T_{max} = 1733\,\mathrm{K}$ and the following combinations of the heating rate h and the holding time t_{hold}:

- ($h = 100\,\mathrm{K\,min^{-1}}$, $t_{hold} = 1\,\mathrm{min}$) yields a relative density of 98 % and large grains with a size of 1.0 ± 0.1 µm, see Fig. 2b.
- ($h = 200\,\mathrm{K\,min^{-1}}$, $t_{hold} = 1\,\mathrm{min}$) yields a relative density of 99 % and medium grains with a size of 0.33 ± 0.03 µm, see Fig. 2c.
- ($h = 200\,\mathrm{K\,min^{-1}}$, $t_{hold} = 0\,\mathrm{min}$) yields a relative density of 99 % and small grains with a size of 0.23 ± 0.03 µm, see Fig. 2d.

The oxide structure after oxidation for 44 h is shown in Fig. 2f,g. The sample with large grains forms an oxide layer with a thickness of 8 µm, see Fig. 2f. On top there is a 0.5 µm thick W--Y--O layer, almost fully covering the 0.3 µm thick Cr_2O_3 layer. Underneath, there is a thick, porous W--Cr--O layer. In contrast, the sample with small grains formed a closed, protective Cr_2O_3 layer with an average thickness $d = 1.3 \pm 0.3\,\mu\mathrm{m}$, as shown in Fig. 2g. The surface roughness (R_a), measured with the profilometer Dektak 6M (see section 2), is

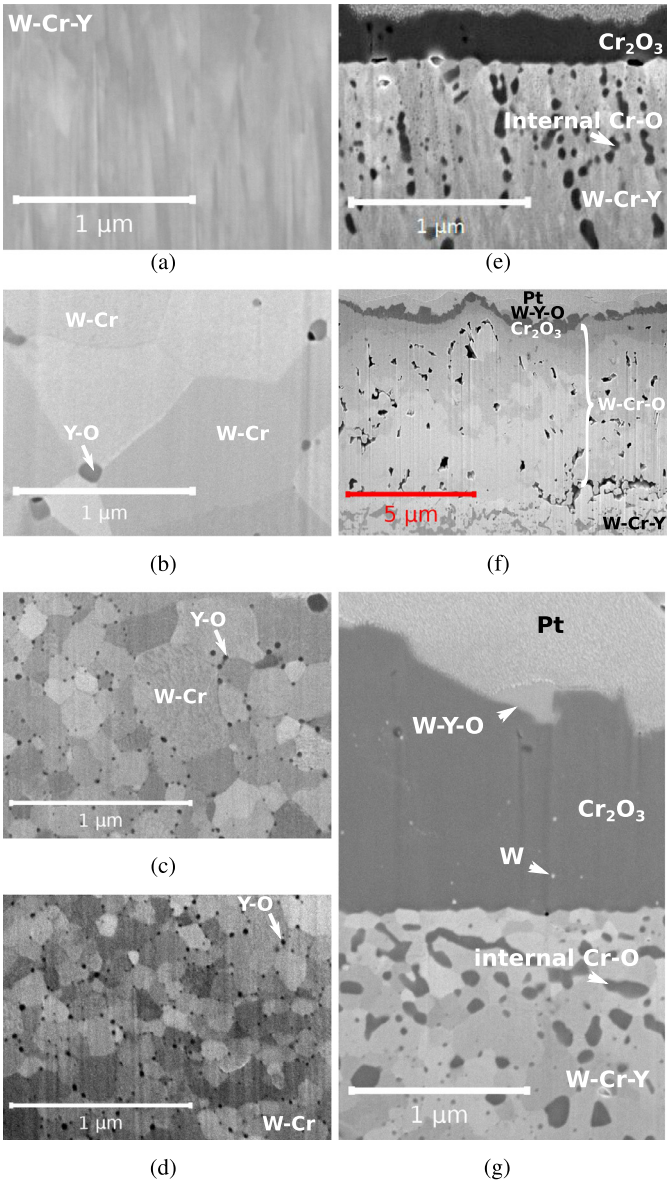

Fig. 2. Electron microscopy images of cross sections. (a)–(d) show the microstructure before oxidation. (a) is a thin film prepared by magnetron sputtering. (b)–(d) are bulk samples where (b) has large grains, (c) medium grains, and (d) small grains. (e)–(g) show the microstructure after oxidation at a temperature of 1273 K at 20 kPa O_2 and 80 kPa Ar partial pressure. (e) shows sample (a) after 75 min of oxidation. (f) shows sample (b) after 44 h of oxidation. (g) shows sample (d) after 44 h of oxidation.

approximately 0.3 µm. Within the Cr_2O_3 layer there are few white particles with a size of around 20 nm. They are identified as W by EDX. Further, there is internal oxidation as Cr_2O_3 particles form within the metal. On top of the Cr_2O_3 layer, there are a few spots with W--Y--O, potentially also containing a few weight-% of Cr. An example is shown in Fig. 2g. The surface coverage of these oxides is determined by EDX and imaging using an energy selective backscattered detector. It is about 4 % in the centre of the sample. At the edge of the sample, within ~ 0.1 mm from the sharp corners, there is mostly W-containing oxides.

The mass gain due to oxidation at 1273 K in 20 kPa O_2 and 80 kPa Ar partial pressure is shown in Fig. 3. As expected from the thickness of the oxide layers, the sample with the small grains exhibits the lowest mass gain. In contrast, the samples with medium and large grains exhibit larger mass gains.

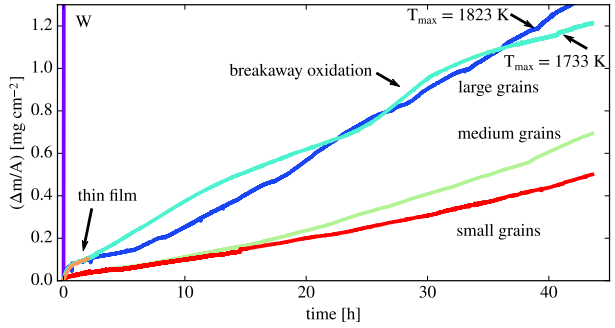

Fig. 3. Mass change of a W-11.4Cr-0.6Y alloy and pure W as a function of time. Measurements are performed at a temperature of 1273 K at 20 kPa O_2 and 80 kPa Ar partial pressure. The samples are produced using different FAST parameters, except for pure W and the thin film which is produced by magnetron sputtering. The corresponding microstructure is shown in Fig. 2.

3.2. Influence of surface roughness on oxidation resistance

After optimisation of the grain structure it is important to understand the relevance of the sample morphology. For that purpose three samples with the small grains are ground differently:

1. The rough sample is obtained with a surface finish using P180-grade silicon carbide abrasive paper. The surface roughness of the sample is $R_a = 0.6 \pm 0.1$ µm.
2. The round sample is obtained with a surface finish using P1200-grade silicon carbide abrasive paper, the surface roughness of the sample is $R_a = 0.04 \pm 0.01$ µm. The sample is ground manually using a planar grinding and polishing machine, very sharp edges are removed. However, a perfectly round shape is not achieved.
3. The standard, cubic sample is obtained with a surface finish using P1200-grade silicon carbide abrasive paper. The surface roughness of the sample is $R_a = 0.04 \pm 0.01$ µm.

Fig. 4 shows that the rough sample oxidises almost twice as fast as the round sample which oxidises almost four times faster than the standard, cubic sample. The detailed evaluation follows in paragraph 4.2.

3.3. Sublimation measurement and life-time studies

In section 3.1 it is shown that samples with small grains can maintain the protective oxide layer for at least two days. However, for full passive safety of a future fusion power plant, it is required that the alloy maintains the protective oxide layer for several weeks to suppress sublimation. In this section the results on the oxidation and sublimation

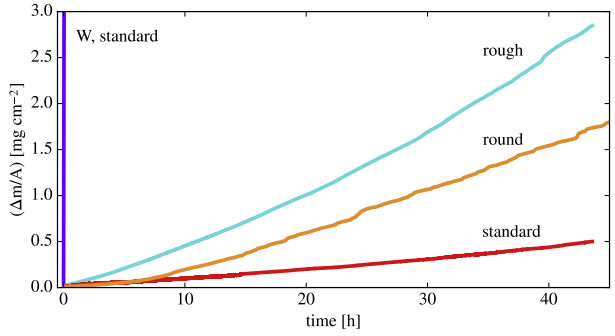

Fig. 4. Mass change of a W-11.4Cr-0.6Y alloy and pure W as a function of time. Measurements are preformed at a temperature of 1273 K at 20 kPa O_2 and 80 kPa Ar partial pressure. The surface finish of the alloys is different, else they are identical.

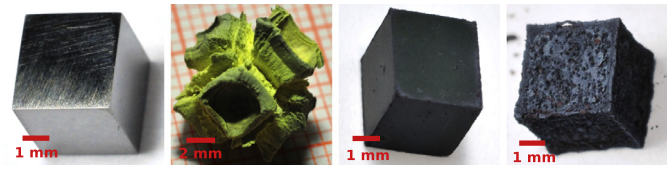

Fig. 5. Photographs of the samples. (a) W–Cr–Y alloy before oxidation after grinding. The pure W samples look the same. (b) Pure W sample after 10 h of oxidation in synthetic air at 1273 K. (c) Optimized W–Cr–Y alloy after 44 h of oxidation in synthetic air at 1273 K. (d) W–Cr–Y alloy after 467 h of oxidation in synthetic air at 1273 K.

performance at 1273 K in synthetic air (20 kPa O_2 and 80 kPaN_2) for up to three weeks of a sample with small grains and a surface finish using P1200-grade silicon carbide abrasive paper are shown. In particular the sublimation measurement, which is performed for the first time, is crucial for qualification of the material.

The photographs, Fig. 5, show the evolution of the samples. Fig. 5a shows the ground cube samples (both the alloy and pure W) before oxidation. Fig. 5b shows a pure W sample after oxidation for 10 h. Volumetric expansion and shape deformation are observed. Fig. 5c,d show smart alloys after oxidation for 44 h and 467 h, respectively. After 44 h there is slight buckling at the corners of the samples, but overall the initial shape is preserved. After 467 h a porous oxide is found, but the initial shape can still be clearly recognized. The corresponding mass change characteristics are shown in Fig. 6. The total mass change of the sample is shown in the upper part of the figure and is the sum of the contribution from sublimation and oxidation. Pure W shows mass gain at a rate of $6 \times 10^{-3}\,mg\,cm^{-2}\,s^{-1}$. The mass change of the alloy can be split into three sections: The first section of 180 h shows mass gain with a rate of around $6 \times 10^{-6}\,mg\,cm^{-2}\,s^{-1}$. It follows the second section with much faster mass gain of around $2.3 \times 10^{-5}\,mg\,cm^{-2}\,s^{-1}$ for 100 h. The maximum mass gain rate for a duration of 30 min is $2 \times 10^{-4}\,mg\,cm^{-2}\,s^{-1}$. In the third section the mass gain reduces back to around $1.0 \times 10^{-5}\,mg\,cm^{-2}\,s^{-1}$.

The lower part of Fig. 6 shows the contribution from sublimation. The dashed line 'sw' indicates the sublimation rate $7 \times 10^{-6}\,mg\,cm^{-2}\,s^{-1}$ of pure W, which is measured for a duration of 1 h and then extrapolated. The solid line shows the sublimation of the alloy. Sublimation is suppressed for about 50 h. In the second and third section of the oxidation process a linear sublimation rate of $1 \times 10^{-6}\,cm^{-2}\,s^{-1}$ is measured.

The results of the microstructure analysis after these 467 h of oxidation at 1273 K are shown in Fig. 7, the surface of the sample in Fig. 7a – W--Cr--O crystals with sizes of up to 5 μm and W--Y--O are found. The

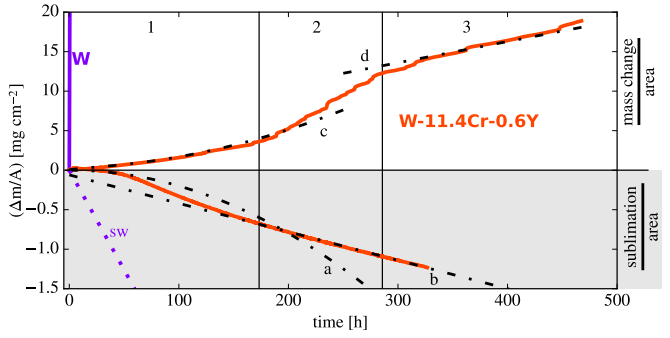

Fig. 6. Mass change of a W-11.4Cr-0.6Y alloy and pure W as a function of time. Measurements are preformed in synthetic air at 1273 K. The upper part shows the total mass change of the sample. The lower part, zoomed-in compared to the upper part, shows the sublimation separately. Stages 1-3 and functions a-d are labelled.

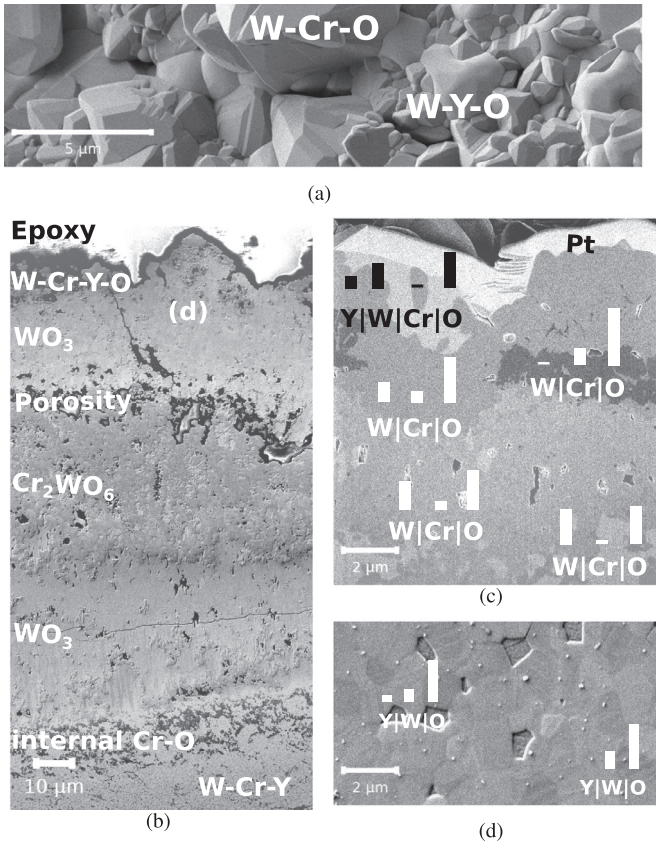

Fig. 7. Electon microscopy of the oxide scale after oxidation of an W-11.4Cr-0.6Y alloy for 467 h at 1273 K in synthetic air. The bars on top of the elements indicate the relative atomic composition measured by EDX. The images show the surface view (a) and the cross section of the full oxide scale (b) where the location of image (d) is marked. The cross section shown in (c) is a FIB cut showing the top 10 μm of the sample.

W--Y--O has a smooth shape without sharp corners. The metallographic cross section of the oxides, Fig. 7b, is obtained by embedding the sample in epoxy, removing the first 2 mm from one side, and polishing. At the surface there are W--Cr--Y-oxides. Below there follow 20 μm of WO_3 with porosity at the interface towards the 31 μm thick Cr_2WO_6 layer. Below the Cr_2WO_6, there is another layer of WO_3 with a thickness of 31 μm before reaching the metal. Internal oxidation of Cr is found within the first 10 μm of the metal. Fig. 7d shows a magnification of the region labelled (d) in Fig. 7b. WO_3 and W-16.8Y-18.4O grains with the equivalent spherical diameter of 0.8 μm are seen.

The first few micrometers are damaged after polishing. Therefore, a FIB cross section, where the surface is protected by a Pt coating, is also performed – see Fig. 7c. Different oxides are found: Cr–O, W--Y--O, and W--Cr--O with Cr content in the range of 3 to 12 weight %.

4. Discussion

4.1. On FAST optimisation

In Section 3.1 it is shown that small grains increase the oxidation resistance, the formation of the protective Cr_2O_3 layer is maintained at least 44 h. The current understanding is as follows: at 1273 K Cr diffuses mainly along the grain boundaries where the vacancy concentration is highest [14]. In the case of larger grains the number of grain boundaries per unit area is smaller. Thus, the total area of grain boundaries is smaller, Cr diffusion is slower and Cr depletion below the oxide scale occurs. This yields the formation of W-containing oxides, see Fig. 2f.

The Pilling Bedworth ratio of WO_3 is 3.4 [7], thus there is a large volumetric expansion. This results in stresses breaking the thin protective Cr_2O_3 layer locally, causing cracking, and breakaway oxidation, see Fig. 3. Cracks allow an faster oxygen supply and locally faster oxidation, thus porosity forms [15]. Further, in the presence of WO_3 and porosity, the protective layer can no longer be replenished and the aim, full passive safety, cannot be accomplished. In case of smaller grains, Cr diffusion is faster. Thus, the Cr supply to replenish the protective scale is maintained longer, see Fig. 2g.

The grain size of the sample is controlled by the FAST sintering parameters. Grain growth mainly occurs at elevated temperatures, the higher the temperature, the faster is the grain growth. Therefore, the time at elevated temperatures should be minimized. This can be achieved by increasing the heating rate h, decreasing the maximum sintering temperature T_{max}, and decreasing the holding time t_{hold}. This is confirmed by the results in Section 3.1. It is a subject of further research to investigate how much further the grain size can be reduced by reducing the time at elevated temperatures while still achieving good densification.

4.2. On the influence of surface roughness on the oxidation

From the cross section in Fig. 3g it is evident that there are four parameters contributing to the mass gain: mass gain due to formation of the Cr_2O_3 layer, mass gain due to internal oxidation, mass gain due to formation of W-containing oxides, and mass loss due to sublimation. A quantification of these contributions is presented in Section 4.3. If the protective Cr_2O_3 layer fails, the formation of W-containing oxides occurs. Thus W-containing oxide formation is more likely to happen at damages and discontinuities of the surface, such as the edge of the sample.

This explains the observations in Fig. 4: the rough sample has many scratches on the surface. Each scratch is a damage of the surface, increasing the probability for failure of the protective Cr_2O_3. Therefore, more W-containing oxides can form (see Fig. 2) and the mass gain increases compared to the standard sample ground with P1200-grade paper. Still, no mass loss is observed (Fig. 4) – that means no oxides detach from the sample and the adhesion of the oxides is given.

The probability of failure of the Cr_2O_3 layer is also increased for the round sample. This is because it is ground hand-held: instead of one discontinuity at the edge of the sample there are many small defects along the rounded corners. Consequently the mass gain is larger compared to the standard sample (Fig. 4).

It is expected that a perfectly round sample exhibits a reduced oxidation rate due to the absence of edges which results in less W-containing oxides. This hypothesis cannot be verified with the existing grinding methods. However, it could be approached using a larger sample as the fraction of the surface in the vicinity of an edge would decrease. The present samples are cubic with a side length of ~ 4 mm.

4.3. On sublimation and life-time studies

In view of the promising results when oxidizing for 2 days, the novel W--Cr--Y alloy with small grains is tested for 3 weeks to approach DEMO-relevant times. The oxidation behaviour shown in Fig. 6 can be understood by estimation of the four contributions to the mass gain Δm_i, $i = 1, 2, 3, 4$:

1. Δm_1 is caused by the formation of the protective Cr_2O_3 layer. This formation is caused by the diffusion of Cr which is described by Fick's first law. Therefore, Δm_1 must follow a parabolic rate law:

$$\Delta m_1/A = \sqrt{c_1 \times t} \tag{1}$$

where A is the surface area of the sample, t the oxidation time, and c_1 a constant. Using a Cr_2O_3 density of $\rho = 5.2\,\mathrm{g\,cm^{-3}}$, $\Delta m_1/A$ can be transformed to the thickness of the Cr_2O_3 layer. After 44 h the Cr_2O_3 layer is intact and the thickness is measured at a cross section. With Eq. (1) this yields $c_1 = 6 \times 10^{-7}\,\mathrm{mg^2\,cm^{-4}\,s^{-1}}$.

2. Δm_2 is caused by the formation of internal Cr_2O_3. This formation is caused by the diffusion of O which is described by Fick's first law. Therefore, Δm_2 must follow a parabolic rate law:

$$\Delta m_2/A = \sqrt{c_2 \times t} \tag{2}$$

where c_2 is a constant. The area covered by internal oxidation is measured on a cross section after 44 h of oxidation. Knowing the sample dimensions and assuming isotropy of the internal oxide this yields a total volume of internal Cr_2O_3 and thus a mass increase Δm_2. With Eq. (2) this yields $c_2 = 9 \times 10^{-8}\,\mathrm{mg^2\,cm^{-4}\,s^{-1}}$.

3. Δm_3 is caused by formation of W-containing oxides, typically at spots where the protective oxide layer failed. Failure of the protective oxide and penetration of W through the protective oxide occurs with a certain probability p. Thus, the area A' covered by W-containing oxides is given by

$$A'(t) = A \times p. \tag{3}$$

At the end of the first oxidation stage, in Fig. 6 after 180 h, the entire sample is effected by failure spots and $A'(t > 180\,\mathrm{h}) = A$

$$\Rightarrow p = \begin{cases} \frac{1}{180\,\mathrm{h}} \times t\,, & t < 180\,\mathrm{h} \\ 1\,, & t > 180\,\mathrm{h} \end{cases} \tag{4}$$

Δm_3 is calculated using this understanding and the oxidation rate of mixed oxides c_3:

$$\Delta m_3 = c_3 \times t \times A'(t) \tag{5}$$

4. Δm_4 is the mass loss caused by sublimation of W-containing oxide with the sublimation rate s, the key to assess the improved safety of the power plant:

$$\Delta m_4 = s \times t \times A'(t) \tag{6}$$

Fitting to the data in Fig. 6 yields $s = -1 \times 10^{-6}\,\mathrm{mg\,cm^{-2}\,s^{-1}}$, the dashed line 'b'. $c_3 = 6 \times 10^{-6}\,\mathrm{mg\,cm^{-2}\,s^{-1}}$ is another fit parameter, so that the model described above yields the calculation of the dashed lines 'a', 'c', and 'd' in Fig. 6. For the dashed line 'd' an additional offset of $5\,\mathrm{mg\,cm^{-2}}$ is required as the second section of the oxidation process is not described by this model. The hypothesis is that there builds up a slight Cr depletion under the protective oxide layer during the first section. This accelerates the oxidation in the second stage of the oxidation process, see Fig. 6.

The goal of suppression of sublimation to avoid radioactive contamination of the environment in case of a LOCA is not fully achieved, Eq. (6) describes the sublimation. This means that there is very little release within the first two days. Later, sublimation with the rate s is found. For a reactor with a first wall surface of $1000\,\mathrm{m^2}$ this implies a potential release of 21 kg with an activity of 1×10^{16} Bq per month. These numbers apply for dry air, in humid air the release could be 10 times higher [16]. However, even in dry air, this is a severe hazard for the environment, in comparison the total release due to the nuclear accident in Fukushima was 5.2×10^{17} Bq, excluding noble gases [17]. However, it should be remarked that one could solve the problem with smart alloys if the cooling was switched back on. With pure W this would not be possible as the first wall would be mechanically destroyed as one can imagine from the photograph shown in Fig. 5b.

The oxidation time in the experiment presented in Fig. 7 is sufficiently long to form oxides according to the phase diagram [18]. That implies that in the presence of W-containing oxides the initially formed Cr_2O_3 layer degrades into WO_3 and Cr_2WO_6. The Y does not form a

stoichiometric oxide with the W, instead it approaches W-14Y-20.8O, which should only form in a molten phase starting from 1427 K. According to the phase diagram [19], this is the solution with the lowest melting point. Thus, the sample is at around 90 % of the melting point of that phase during the experiment. This explains why, the W--Y--O on the surface of the sample, Fig. 7a has a molten-like shape. In order to suppress the sublimation, future developments should attempt to suppress the formation of this compound.

5. Conclusion and outlook

W is a promising candidate as plasma facing armour material for future fusion power plants. Oxidation and sublimation is a major problem in case of air ingress during a LOCA. W--Cr--Y alloys are suggested to avoid a complete mechanical destruction of the first wall and to avoid radioactive contamination of the environment. It is found that the sintering should be optimized towards small grains. Further, it is crucial to have a smooth surface. With submicron grains and a roughness $R_a = 0.04$ µm the formation of a protective Cr_2O_3 layer and suppression of sublimation for two days at 1273 K is shown – this is a major improvement compared to the 8.5 h shown in previous works [6]. Complete mechanical destruction can be avoided successfully – this is tested for the DEMO-relevant timescale of three weeks. However, after more than two days sublimation of W-oxides is measured and the goal of full passive safety is not achieved yet. It would be required to restart cooling. Therefore, the development of advanced W-alloys must continue. One option for further optimisation is to attempt to further reduce the grain size. Another option is to investigate other or additional active elements, such as Zr, to further support the formation of a protective Cr_2O_3 layer.

Acknowledgments

A part of this work has been carried out within the framework of the EUROfusion Consortium and has received funding from the Euratom research and training programme 2014–2018 under grant agreement No. 633053. The views and opinions expressed herein do not necessarily reflect those of the European Commission.

References

[1] J.W. Coenen, S. Antusch, M. Aumann, et al., Materials for DEMO and reactor applications-boundary conditions and new concepts, Phys. Scr. 2016 (T167) (2016) 014002.
[2] Y. Ueda, K. Schmid, M. Balden, et al., Baseline high heat flux and plasma facing materials for fusion, Nucl. Fusion 57 (9) (2017) 092006.
[3] Ch. Linsmeier, et al., Development of advanced high heat flux and plasma-facing materials, Nucl. Fusion 57 (9) (2017) 092007.
[4] M.R. Gilbert, J.-C. Sublet, R.A. Forrest, Handbook of activation, transmutation, and radiation damage properties of the elements simulated using FISPACT-II & TENDL, Culham Center For Fusion Energy, 2015.
[5] D. Maisonnier, I. Cook, et al., The European power plant conceptual study, Fusion Eng. Des. (75–79) (2005) 1173–1179.
[6] T. Wegener, F. Klein, A. Litnovsky, et al., Development and analyses of self-passivating tungsten alloys for DEMO accidental conditions, Fusion Eng. Des. 124 (C) (2017) 183–186.
[7] J.R. Davis (Ed.), ASM Specialty Handbook: Heat-Resistant Materials, S. D. Henry, 1999.
[8] T. Wegener, F. Klein, A. Litnovsky, et al., Development of yttrium-containing self-passivating tungsten alloys for future fusion power plant, Nuclear Mater. Energy 9 (2016) 394–398.
[9] A. Litnovsky, T. Wegener, F. Klein, et al., New oxidation-resistant tungsten alloys for use in the nuclear fusion reactors, Phys. Scr. T170 (014012) (2017).
[10] A. Litnovsky, T. Wegener, F. Klein, et al., Advanced smart tungsten alloys for a future fusion power plant, Plasma Phys. Control. Fusion 59 (2017) 064003.
[11] O. Guillon, J. Gonzalez-Julian, B. Dargatz, et al., Field-assisted sintering technology/spark plasma sintering: mechanisms, materials, and technology developments, Adv. Eng. Mater. 16 (7) (2014) 830–849.
[12] A. Calvo, C. Garcia-Rosales, F. Koch, et al., Manufacturing and testing of self-passivating tungsten alloys of different composition, Nuclear Mater. Energy 9 (2016) 422–429.
[13] S. Telu, R. Mitra, S.K. Pabi, Effect of Y_2O_3 addition on oxidation behavior of W-Cr alloys, Metallur. Mater. Trans. A 46 (12) (2015) 5909–5919.
[14] F.J.A. Den Broeder, Interface reation and a special form of grain boundary diffusion in the Cr-W system, Acta Metallurgica 20 (3) (1972) 319–332.
[15] S.C Cifuentes, et al., On the oxidation mechanism of pure tungsten in the temperature range 600 – 800°C, Corros. Sci. 57 (2012) 114–121.
[16] A. Litnovsky, F. Klein, T. Wegener, et al., Smart first wall materials for intrinsic safety of a future power plant, ISFNT-13, Kyoto, Japan, 25 Sep 2017 – 29 Sep 2017, (2017).
[17] G. Steinhauser, A. Brandl, T.E. Johnson, Comparison of the chernobyl and fukushima nuclear accidents: a review of the environmental impacts, Sci. Total Environ. 470–471 (2014) 800–817.
[18] K.T. Jacob, Phase relationships in the system Cr-W-O and thermodynamic properties of $CrWO_4$ and Cr_2WO_4, J. Mater. Sci. 15 (9) (1980) 2167–2174.
[19] H.J. Borchardt, Yttrium-tungsten oxides, Inorg. Chem. 2 (1) (1963) 170–173.